Nonlocal Desorption of Chlorobenzene Molecules from the Si(111)-(7 × 7) Surface by Charge Injection from the Tip of a Scanning Tunneling Microscope: Remote Control of Atomic Manipulation

P. A. Sloan, S. Sakulsermsuk, and R. E. Palmer

Nanoscale Physics Research Laboratory, School of Physics and Astronomy, University of Birmingham, Birmingham, B15 2TT, United Kingdom

(Received 9 December 2009; published 19 July 2010)

We report the nonlocal desorption of chlorobenzene molecules from the Si(111)-(7 × 7) surface by charge injection from the laterally distant tip of a scanning tunneling microscope and demonstrate remote control of the manipulation process by precise selection of the atomic site for injection. Nonlocal desorption decays exponentially as a function of radial distance (decay length ~100 Å) from the injection site. Electron injection at corner-hole and faulted middle adatoms sites couples preferentially to the desorption of distant adsorbate molecules. Molecules on the faulted half of the unit cell desorb with higher probability than those on the unfaulted half.

DOI: 10.1103/PhysRevLett.105.048301 PACS numbers: 82.37.Gk, 68.37.Ef, 68.43.Rs, 73.20.−r

The manipulation of individual atoms with the scanning tunneling microscope (STM) represents a fundamental boundary of materials control [1–6]. If, in some hypothetical future, atomic manipulation were ever to become a practical technique for device fabrication, one (or both) of two radical developments would probably be required: (i) parallelization of the process, e.g., via microfabricated arrays of STM tips, and/or (ii) remote control, in the sense of atomic manipulation events initiated at many locations distant from a given STM tip. ''Remote control'' requires us to both (a) identify and (b) master nonlocal processes initiated by charge injection. Regarding (a), the first examples of nonlocal manipulation have now been observed on metal and semiconductor surfaces. The present work is the first step towards (b), in that it demonstrates how the cross section for a remote manipulation event depends delicately on the STM charge injection site, with atomic precision. Furthermore, our results also have striking implications for the absolute cross sections for a whole raft of published STM scanning [7–12] (versus local [5]) manipulation experiments as well as electron-beam [13,14] and photoinduced surface chemical processes [15], because the possibility of lateral charge transport of the type exploited here has not generally been considered.

Examples of nonlocal STM manipulation [16] include S-S bond breaking in CH_3SSCH_3 molecules hundreds of angstroms from the injection site on the Au(111) surface at 5 K [17] and diffusion or rearrangement of water clusters on the Ag(111) surface [18]. Hydrogenated nanoislands of Co on the Cu(111) surface can be dehydrogenated by charge injection into a particular island while leaving other islands untouched [19]. Nonlocal manipulation by electron and hole injection has been reported for the clean Si(111)-(7 × 7) surface [3] and various adsorbed species, including C_{60} [20], chemisorbed chlorine atoms [21], and physisorbed chlorobenzene molecules [11]. In none of these cases has a dependence on the charge injection site been reported. In this Letter we demonstrate that nonlocal manipulation (specifically desorption) of chemisorbed chlorobenzene molecules on the Si(111)-(7 × 7) surface, via injection of both electrons and holes, depends sensitively not only on voltage but also on the precise choice of charge injection site, i.e., within a unit cell remote from the molecules which desorb (~100 Å away). Molecules on the faulted half of the unit cell desorb with higher probability than those on the unfaulted half.

The experiments were performed at room temperature with an RHK-400 STM in an ultrahigh vacuum chamber with a base pressure of 6×10^{-11} Torr. Tungsten tips were etched by the dropoff technique using a circular gold anode in 2*M* NaOH solution with a bias of 9 V. Tungsten-oxide was removed by resistive heating in high vacuum. Silicon samples were cut from phosphorous-doped *n*-type (1–30 Ω cm) wafers of Si(111), degassed at ~600 °C in the UHV chamber for a few hours before ''flashing,'' typically for 10 s, to temperatures increasing until 1250 °C. An in-house computer program was used to correlate the exact atomic locations of all molecules in STM images taken before and after charge injection [22]. Typically 1000 molecules were analyzed to obtain each data point in Figs. 2–4 below. From an initial stabilization voltage of +2 V [23], scanning tunneling *I*-*V* spectra (STS) were taken from 0 to +3.5 V with the tunnel gap reduced by 1.18 Å/V to amplify the signal at low voltage. The variable gap *I*-*V* spectra were converted to constant gap (with $\kappa = 1$ Å^{-1}) before numerical differentiation to generate $(dI/dV)/(I/V)$ spectra. The use of the same κ value for all locations may overestimate the $(dI/dV)/(I/V)$ spectra at valley locations on the surface, but should not lead to qualitative changes in the spectra.

Figure 1 shows a pair of STM images taken before 1(a) and after 1(b) injection of electrons at the site marked by the center of an X on the Si(111)-(7 × 7)

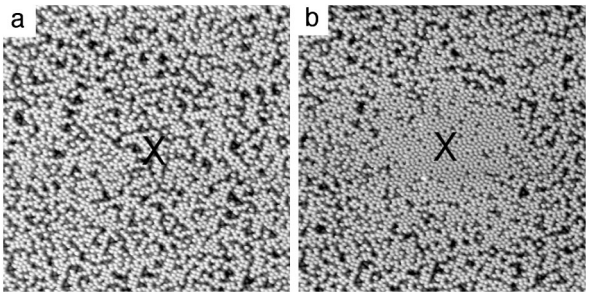

FIG. 1. STM images (+1 V, 250 pA, 512 Å × 512 Å) of a Si(111)-(7 × 7) surface (a) with a large dose of chlorobenzene molecules, which image as missing adatoms, and (b) after charge injection (+3.6 V, 250 pA, 4.46 s) at the site marked with an X in the image. Nonlocal desorption of chlorobenzene molecules remote from the charge injection site is evident.

surface. Figure 1(a) shows a high dose, ~5 molecules per unit cell (maximum 6), of chemisorbed chlorobenzene molecules (which appear as missing silicon adatoms). After electron injection (+ 3.6 V, 250 pA, 4.46 s, feedback loop on), Fig. 1(b) shows that an area ~150 Å in radius surrounding the injection site is depopulated of chlorobenzene molecules. Increasing the duration, current, or voltage of the injection pulse increased the size of the depopulated area. We were able to depopulate areas ~500 Å in radius with no upper limit found. This nonlocal desorption was found for both injection of electrons and holes. Neither grain boundaries nor steps in the surface blocked the process.

To capture quantitatively the probability of manipulation (desorption) per electron, the differential equation $dN(r)/dt = -k_e N(r)a(r)$ is used to describe the rate of change of the population $N(r)$ of an annulus at radius r from the injection site. The number of electrons (or holes) that impinge upon an individual molecule at radius r is $a(r)$, and the probability per impinging electron (or hole) of causing a desorption event is k_e. The current density $a(r)$ will of course decrease geometrically as $1/2\pi r$ as charge flows away from the injection site. Assuming a linear cross section for a single molecule of L, the number of injected electrons that then impinge on a molecule per second at a distance r is given by $a(r) = (sIL/e2\pi r)f(r)$, where s is the (unknown) fraction of the injection current I that initially flows across the surface, e is the electron charge, and $f(r)$ describes the radial decay of the surface current (e.g., by inelastic scattering). We take L to be 5 Å. The fraction s might in principle be derived from the ratio of surface to bulk conductivity for Si(111)-(7 × 7), but reported values of the surface conductivity vary widely [24]; as with L, the value of s does not affect the qualitative dependence on voltage, current, etc., so for simplicity we use $s = 1$. Integrating the rate equation over the duration t of the injection pulse gives, $k_e f(r) = -e2\pi r \ln[N(r)/N_0(r)]/stIL$, where $N_0(r)$ is the population of the annulus at radius r before injection and $N(r)$ is the number of molecules that retain their original position (i.e., do not diffuse or desorb) after injection. The data are corrected for thermally induced desorption and displacement, ~5% of events, before plotting [22].

Figure 2 presents $k_e f(r)$ as a function of radial distance from the site of charge injection at +2.7 V. The decay is fitted with a single exponential $k_e \exp(-r/\lambda)$ with best fit parameters of $k_e = (3.80 \pm 0.05) \times 10^{-9}$ and decay length λ of (74.7 ± 3.4) Å. Below ~50 Å radius the exponential function does not fit the experimental data, and these data points are omitted from the fit. We found no appreciable change of the decay length with coverage of chlorobenzene in the range 2–4 molecules per unit cell. To confirm that the injected *current* drives the nonlocal desorption, and thus rule out electric-field effects and mechanical tip or sample interactions, Fig. 2(b) shows a family of nonlocal decay curves taken with the same injection voltage and total charge dose, but with different tunneling currents and injection times. Our analysis assumes a one electron (or hole) process and should therefore be invariant to the tunneling current or time, as Fig. 2(b) confirms. Following an analysis similar to Ref. [17], we calculate the number of electrons per nonlocal desorption event as 0.90 ± 0.03. This matches well with our previous

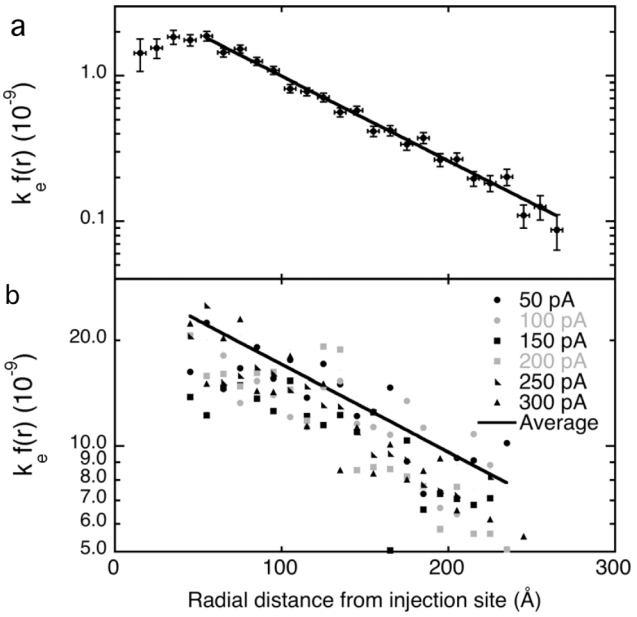

FIG. 2. (a) Nonlocal desorption probability as a function of radial distance from site of injection (at +2.7 V). Error bars reflect the 10 Å width of the annulus used in the analysis and the standard deviation on the mean assuming a Poisson distribution for the number of molecules before and after injection. The (best) fit is a single exponential decay, $k_e \exp(-r/\lambda)$ with $k_e = (3.80 \pm 0.05) \times 10^{-9}$ and $\lambda = (74.7 \pm 3.4)$ Å. Points closer than 50 Å from the injection site are omitted from the fit (see text for details). (b) As for (a) but for six different tunneling currents and injection voltage of +3.6 V. The total charge dose was kept approximately constant by varying the duration of the injection pulse: 50 pA/37.8 s, 100 pA/18.9 s, 150 pA/12.8 s, 200 pA/10 s, 250 pA/7.5 s, 300 pA/6.3 s.

measurement using the scanning method of 0.88 ± 0.09 [9].

Figure 3(a) presents the most important result of this work, the probability of nonlocal desorption per injected electron (at +2.7 V) as a function of injection site across a Si(111)-(7 × 7) unit cell. The data were obtained by placing the STM tip at a series of atomic locations along a line joining one corner-hole site to the opposite corner-hole site [Fig. 3(b)]. Broadly, electron injection into the faulted half of the cell yields more efficient nonlocal desorption. The sensitivity of the nonlocal desorption process to the precise atomic location of the injection site is evident; the corner-hole and faulted middle adatom sites most favor desorption. How does the observed site-dependent nonlocal desorption probability map onto the electronic structure of the surface? The voltage chosen in Fig. 3(a), +2.7 V, is the second threshold in the desorption probability, the first is at +2.1 V [9]. The STM populates electronic states from the injection voltage down to the Fermi level with appropriate weighting for the tunneling probability. Thus, nonlocal desorption at +2.7 V should be dominated by the feature that causes the +2.1 V threshold.

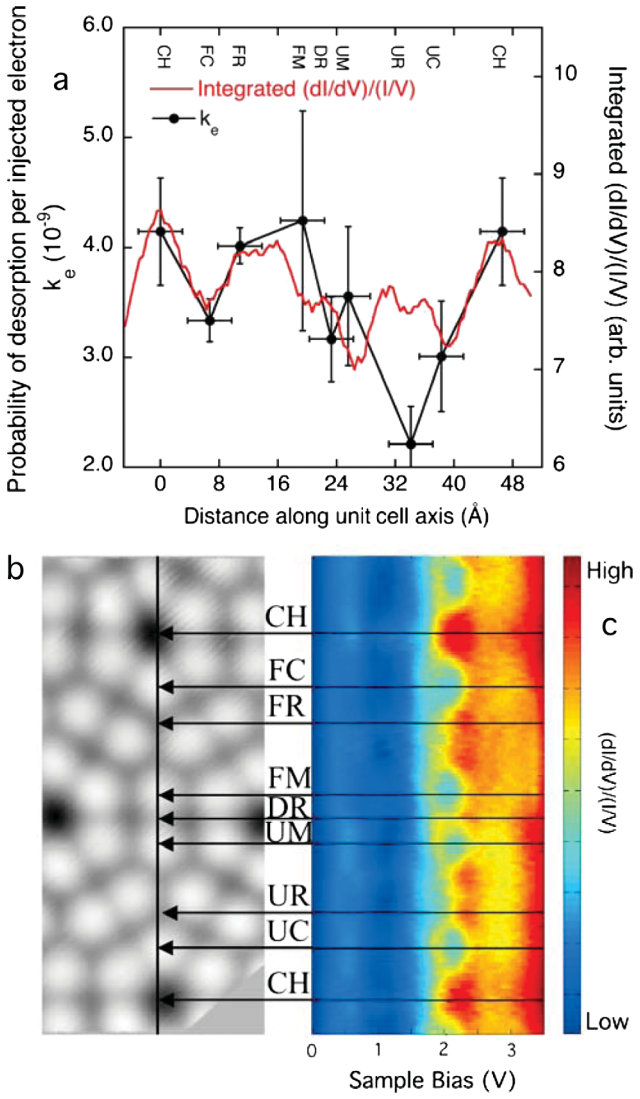

FIG. 3 (color). Site-specific nonlocal atomic manipulation. (a) Probability per electron (injected at +2.7 V, 800 pA with pulse duration of 8 s) of nonlocal desorption of chlorobenzene molecules for seven distinct atomic injection sites on the Si(111)-(7 × 7) surface: CH, corner-hole; FC, faulted corner adatom; FR, faulted rest atom; FM, faulted middle adatom; DR, dimer row; UM, unfaulted-middle adatom; UR, unfaulted rest atom; UC, unfaulted corner adatom, as labeled in the +1 V STM image, (b). (c) STS map of the Si(111)-(7 × 7) surface along the line indicated in (b). A section through the data in (c) integrated with appropriate weighting from +2.0 to +2.7 V is also plotted in (a) for comparison with the desorption results.

To understand better the delicate dependence of the nonlocal desorption dynamics on the (remote) atomic site where charge is injected, we also measured 128 equally spaced scanning tunneling spectra along the same high symmetry line [Fig. 3(b)], from corner hole to corner hole, which are proportional to the local density of states (LDOS). Figure 3(c) shows the corresponding $(dI/dV)/(I/V)$ map generated from an average of 4096 $(dI/dV)/(I/V)$ spectra. For the unoccupied states (positive bias), the +0.5 V dangling bond ("U_1") state associated with the adatoms is evident. The main electronic feature found above this is the "U_2 backbond" state at +1.6 V [25]. Both these states lie below the threshold for desorption at +2.1 V. However, we also find a new state at $\sim +2.1$ V that is predominantly located at the corner-hole (especially) and rest atom sites (faulted rest atom and unfaulted rest atom) rather than at the adatom sites. This is the threshold surface state for nonlocal desorption. Increasing the voltage in Fig. 3(c) to +2.7 V, to match the desorption experiment voltage, sees the predominance of the corner-hole retained in the LDOS and a relative suppression of the rest atom sites, in line with the desorption probability. The observed correlation, Fig. 3(a), between the injected site-dependent nonlocal desorption probability and the density of states integrated from +2.0 to +2.7 V demonstrates that the site dependence arises from the coupling of the STM tip to the surface state in which the carriers (here electrons) are transported across the surface before they induce molecular desorption. Moreover, the prominence of the corner-hole site in the data suggests that electrons may be transported in a state lying spatially below the topmost adatom layer of the surface, since the corner-hole atoms lie in the fourth layer of the crystal. Such a "subsurface" state may also explain the insensitivity of the nonlocal desorption to surface steps, which is not observed for lateral charge transport in the first layer adatom surface states [26].

The probability of nonlocal desorption depends not only on the charge injection site but also on the molecular adsorption site. Figure 4(a) shows that, taking an average over injection sites, molecules on the faulted side of the unit cell are more likely to desorb than those on the unfaulted side. This matches the integrated LDOS from 2 to 2.7 V over the faulted and unfaulted halves of the unit

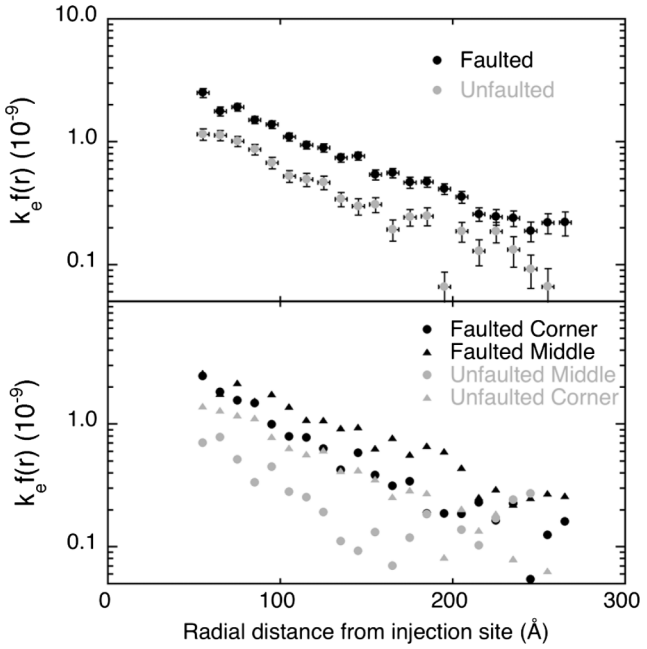

FIG. 4. Nonlocal desorption at +2.7 V as a function of molecular adsorption site. (a) Comparison of molecules on the faulted (black circles) and unfaulted (gray circles) halves of the Si(111)-(7 × 7) unit cell. (b) Molecules on the four specific adatom sites in the Si(111)-(7 × 7) unit cell: faulted corner (black circles), faulted middle (black triangle), unfaulted middle (gray circle), and unfaulted corner (gray triangle).

cell, Fig. 3(a). However, the di-σ bonding [27] to an adatom and rest atom pair will necessarily distort the LDOS with respect to the clean surface; thus the clean surface LDOS may not reflect the LDOS at the adsorbate site. Figure 4(b) shows the results for the four adsorption sites of chlorobenzene on the Si(111)-(7 × 7) surface, faulted corner, faulted middle, unfaulted corner, and unfaulted middle. All the molecular sites show similar probability for desorption apart from the unfaulted middle, where the probability is much lower. This adsorption site sensitivity of the nonlocal desorption process presumably reflects the coupling of the propagating surface state(s) to the resonant electronic state of the chemisorbed molecule that drives desorption. We hope that the present experimental work will provoke advanced theoretical treatments of the interaction between electronic charge injection, scattering, and coupling to the nonadiabatic dynamics.

Finally, we remark that the type of nonlocal molecular manipulation process analysis herein has implications for both atomic manipulation and surface electron beam and photochemistry on the Si(111)-(7 × 7) and other surfaces. (1) Threshold voltages or energies may depend on the surface electronic states and not the molecular adsorbate states as is generally assumed. We find that the molecular threshold for desorption effectively acts as a high-pass energy filter, selecting which current propagating surface state can couple to molecular manipulation, e.g., rejecting the U_1 and U_2 surface states. (2) The probability of manipulation per electron extracted from STM scanning experiments here overestimates the true probability by nearly 2 orders of magnitude. This will impact the resonance state lifetimes required to generate a given manipulation probability in calculations [8,28], which sometimes seem unfeasibly large. The same consideration applies to processes driven by photoelectrons or secondary electrons [15]. Looking ahead, site-specific control of nonlocal manipulation suggests new routes to the control of large scale atomic manipulation via surface-state control.

We thank the EPSRC for funding this research. S. S. is grateful to the Thailand Frontier Research Network for financial support.

[1] D. M. Eigler and E. K. Schweizer, Nature (London) **344**, 524 (1990).
[2] G. P. Salam, M. Persson, and R. E. Palmer, Phys. Rev. B **49**, 10 655 (1994).
[3] B. C. Stipe, M. A. Rezaei, and W. Ho, Phys. Rev. Lett. **79**, 4397 (1997).
[4] J. I. Pascual *et al.*, Nature (London) **423**, 525 (2003).
[5] L. Soukiassian *et al.*, Phys. Rev. B **68**, 035303 (2003).
[6] P. A. Sloan and R. E. Palmer, Nature (London) **434**, 367 (2005).
[7] P. H. Lu, J. C. Polanyi, and D. Rogers, J. Chem. Phys. **111**, 9905 (1999).
[8] S. Alavi *et al.*, Phys. Rev. Lett. **85**, 5372 (2000).
[9] P. A. Sloan *et al.*, Phys. Rev. Lett. **91**, 118301 (2003).
[10] P. A. Sloan and R. E. Palmer, Nano Lett. **5**, 835 (2005).
[11] X. K. Lu, J. C. Polanyi, and J. Yang, Nano Lett. **6**, 809 (2006).
[12] P. A. Sloan and R. E. Palmer, J. Phys. Condens. Matter **18**, S1873 (2006).
[13] R. E. Palmer, Prog. Surf. Sci. **41**, 51 (1992).
[14] R. E. Palmer and P. J. Rous, Rev. Mod. Phys. **64**, 383 (1992).
[15] P. V. Kamat, Chem. Rev. **93**, 267 (1993).
[16] J. M. MacLeod *et al.*, ACS Nano **3**, 3347 (2009).
[17] P. Maksymovych *et al.*, Phys. Rev. Lett. **99**, 016101 (2007).
[18] H. Gawronski *et al.*, Phys. Rev. Lett. **101**, 136102 (2008).
[19] M. Sicot *et al.*, Phys. Rev. B **77**, 035417 (2008).
[20] K. Maeda and Y. Nakamura, Surf. Sci. **528**, 110 (2003).
[21] Y. Nakamura, Y. Mera, and K. Maeda, Phys. Rev. Lett. **89**, 266805 (2002).
[22] S. Sakulsermsuk *et al.*, J. Phys. Condens. Matter **22**, 084002 (2010).
[23] R. J. Hamers, R. M. Tromp, and J. E. Demuth, Phys. Rev. Lett. **56**, 1972 (1986).
[24] P. Hofmann and J. W. Wells, J. Phys. Condens. Matter **21**, 013003 (2009).
[25] R. Wolkow and P. Avouris, Phys. Rev. Lett. **60**, 1049 (1988).
[26] S. Heike *et al.*, Phys. Rev. Lett. **81**, 890 (1998).
[27] Y. Cao, J. F. Deng, and G. Q. Xu, J. Chem. Phys. **112**, 4759 (2000).
[28] N. L. Yoder *et al.*, Phys. Rev. Lett. **97**, 187601 (2006).